RIM genes differentially contribute to organizing presynaptic release sites

Pascal S. Kaeser[a,b,1,2], Lunbin Deng[a,1,3], Mingming Fan[a,1], and Thomas C. Südhof[a,2]

[a]Department of Molecular and Cellular Physiology, and Howard Hughes Medical Institute, Stanford University School of Medicine, Stanford, CA 94304-5453; and [b]Department of Neurobiology, Harvard Medical School, Boston, MA 02115

Contributed by Thomas C. Südhof, June 2, 2012 (sent for review May 4, 2012)

Tight coupling of Ca^{2+} channels to the presynaptic active zone is critical for fast synchronous neurotransmitter release. RIMs are multidomain proteins that tether Ca^{2+} channels to active zones, dock and prime synaptic vesicles for release, and mediate presynaptic plasticity. Here, we use conditional knockout mice targeting all RIM isoforms expressed by the *Rims1* and *Rims2* genes to examine the contributions and mechanism of action of different RIMs in neurotransmitter release. We show that acute single deletions of each *Rims* gene decreased release and impaired vesicle priming but did not alter the extracellular Ca^{2+}-responsiveness of release (which for *Rims* gene mutants is a measure of presynaptic Ca^{2+} influx). Moreover, single deletions did not affect the synchronization of release (which depends on the close proximity of Ca^{2+} channels to release sites). In contrast, deletion of both *Rims* genes severely impaired the Ca^{2+} responsiveness and synchronization of release. RIM proteins may act on Ca^{2+} channels in two modes: They tether Ca^{2+} channels to active zones, and they directly modulate Ca^{2+}-channel inactivation. The first mechanism is essential for localizing presynaptic Ca^{2+} influx to nerve terminals, but the role of the second mechanism remains unknown. Strikingly, we find that although the RIM2 C_2B domain by itself significantly decreased Ca^{2+}-channel inactivation in transfected HEK293 cells, it did not rescue any aspect of the RIM knockout phenotype in cultured neurons. Thus, RIMs primarily act in release as physical Ca^{2+}-channel tethers and not as Ca^{2+}-channel modulators. Different RIM proteins compensate for each other in recruiting Ca^{2+} channels to active zones, but contribute independently and incrementally to vesicle priming.

exocytosis | synapse | Munc13

In a presynaptic nerve terminal, Ca^{2+} triggers synaptic vesicle exocytosis at specialized sites called active zones. Among the major active zone proteins (e.g., RIMs, α-liprins, ELKS's, RIM-BPs, Piccolo/Bassoon, and Munc13's), RIMs stand out because they bind to all other components of active zones and are involved in all central aspects of neurotransmitter release (1, 2). In vertebrates, two RIM genes (*Rims1* and *Rims2*) synthesize five principal RIM isoforms from independent promoters (RIM1α, RIM1β, RIM2α, RIM2β, and RIM2γ; Fig. 1*A*); these isoforms are further diversified by alternative splicing (3–5). Moreover, two additional RIM genes (*Rims3* and *Rims4*) produce only γ-isoforms, which are not further considered here. Gene deletion experiments (Table S1) showed that RIMs are essential for multiple aspects of neurotransmitter release (4, 6–10) and for presynaptic short- and long-term plasticity (4, 6, 11–13). However, how different RIM isoforms contribute to neurotransmitter release is unclear.

Recent studies revealed that RIMs regulate presynaptic Ca^{2+} channels via two independent mechanisms, namely by recruiting Ca^{2+} channels to active zones (14) and by modulating Ca^{2+}-channel opening times (15, 16). The first activity is mediated by a tripartite complex of RIMs, RIM-BPs, and Ca^{2+} channels in which the RIM PDZ domains directly bind to the C-termini of N- and P/Q-type Ca^{2+} channels, the RIM PxxP-sequences bind to RIM-BPs, and RIM-BPs, in turn, directly bind to the C-termini of Ca^{2+} channels (14, 17, 18). The second activity is mediated by the RIM C_2B-domain, possibly by binding to β4 subunits of Ca^{2+} channels (15, 16). However, the relative contributions of different RIM isoforms and of their interactions with Ca^{2+} channels are unknown. In particular, although the Ca^{2+}-channel tethering activity of RIMs was shown to be essential for normal presynaptic Ca^{2+} influx, the physiological role of the Ca^{2+}-channel modulation by RIMs has not been tested.

Here, we have systematically dissected the contributions of (*i*) the *Rims1* and *Rims2* gene products, and (*ii*) the different Ca^{2+}-channel functions of RIM proteins to neurotransmitter release. Using electrophysiological analyses in conditional knockout mice, we demonstrate that both the RIM1 and the RIM2 proteins contribute to neurotransmitter release. Whereas single *Rims1* and *Rims2* deletions alone impaired priming and neurotransmitter release, Ca^{2+} influx as monitored by the Ca^{2+} dependence of release is not affected, but is severely impaired by the double deletion. Moreover, we show that although RIM C_2B domains modulate Ca^{2+}-channel opening in transfected cells in vitro, the loss of this activity does not detectably contribute to the impairment in Ca^{2+} influx and neurotransmitter release caused by the double KO of the *Rims1* and *Rims2* genes in vivo.

Results

Functional Redundancy Among RIM Proteins in Ca^{2+} Influx. Previous studies suggested that RIM proteins redundantly enable synaptic vesicle exocytosis (4, 10), but the extent to which the different RIM isoforms contribute to release has not been established. To address this question, we examined neurotransmitter release in cultured neurons in which the *Rims1* gene encoding RIM1α and RIM1β and the *Rims2* gene encoding RIM2α, RIM2β, and RIM2γ were acutely deleted either alone or together. In these experiments, we restricted our analyses to inhibitory synapses for two reasons: (*i*) we showed that excitatory and inhibitory synaptic transmission are similarly affected in RIM double-deficient neurons (14, 19), suggesting that the phenotype observed in inhibitory synapses likely applies to all synapses; and (*ii*) inhibitory synaptic responses are more precisely analyzed in cultured neurons than excitatory responses because they are not contaminated by recurrent network activity (20).

We cultured primary hippocampal neurons from newborn homozygous conditional *Rims1*, *Rims2*, and double *Rims1*/*2* KO mice (4, 14) and infected the neurons with lentiviruses expressing active or inactive mutant cre-recombinase (referred to as cre and control in all figures). Active and inactive cre were expressed as

Author contributions: P.S.K., L.D., and T.C.S. designed research; P.S.K., L.D., and M.F. performed research; P.S.K., L.D., M.F., and T.C.S. analyzed data; and P.S.K. and T.C.S. wrote the paper.

The authors declare no conflict of interest.

[1]P.S.K., L.D., and M.F. contributed equally to this work.

[2]To whom correspondence may be addressed. E-mail: kaeser@hms.harvard.edu or tcs1@stanford.edu.

[3]Present address: Department of Neuroscience, Genentech, South San Francisco, CA 94080.

This article contains supporting information online at www.pnas.org/lookup/suppl/doi:10.1073/pnas.1209318109/-/DCSupplemental.

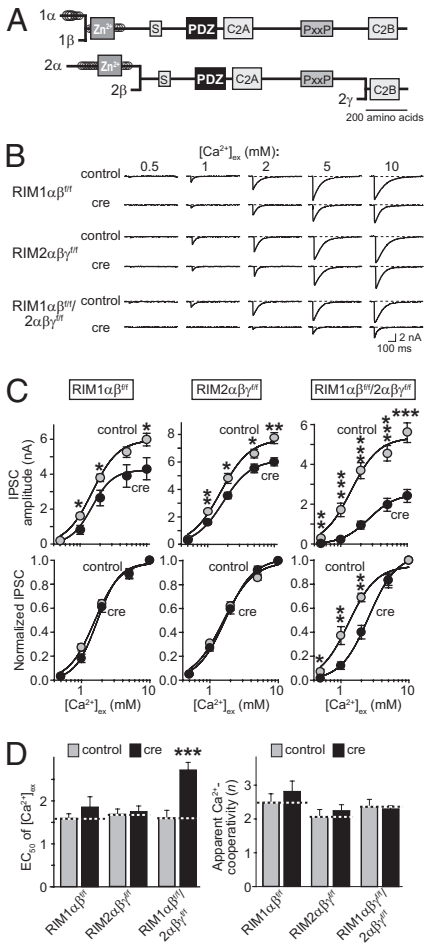

Fig. 1. Comparative analysis of the effects of single and double RIM1α/β and RIM2α/β/γ deletions on the amplitude and Ca^{2+} dependence of neurotransmitter release at inhibitory synapses. Experiments in this and the following figures (except Fig. 4) were performed in cultured hippocampal neurons from conditional floxed RIM1αβ$^{f/f}$, RIM2αβγ$^{f/f}$, and/or double RIM1αβ$^{f/f}$/RIM2αβγ$^{f/f}$ mice that were infected with lentiviruses expressing either active cre-recombinase (cre) or catalytically inactive, mutated cre-recombinase (control). (*A*) Domain structures of RIM proteins encoded by the *Rims1* and *Rims2* genes (Zn, N-terminal zinc finger domain, flanked by α-helical coils; S, serine corresponding to phosphorylatable serine^{413} in RIM1α; PDZ, central PDZ domain; C_2A and C_2B, central and C-terminal C_2 domains, respectively; PxxP, proline-rich sequence). (*B*) Sample traces of IPSCs elicited by focal stimulation in neurons lacking either RIM1α/β or RIM2α/β/γ alone or together at the indicated concentrations of extracellular Ca^{2+} ($[Ca^{2+}]_{ex}$). Each RIM-deficient class of neurons is associated with a separate independent control. (*C*) Summary graphs of absolute (*Upper*) and normalized IPSC amplitudes (*Lower*; normalized to the response at 10 mM $[Ca^{2+}]_{ex}$). The lines correspond to fits of the data to a Hill function (24). (*D*) Summary graphs of the EC_{50} (*Left*; the $[Ca^{2+}]_{ex}$ that elicits 50% of the maximal response) and of the apparent Ca^{2+} cooperativity (*Right*), determined by fitting each single experiment shown in *B* to a Hill function. Data shown are means ± SEMs, statistical significance (*$P < 0.05$; **$P < 0.01$; ***$P < 0.001$) was determined by one-way ANOVA (*C*) or Student's *t* test (*D*). RIM1αβ$^{f/f}$: control, n = 9 cells in 3 independent batches of cultures; cre, n = 10/3; RIM2αβγ$^{f/f}$: control, n = 7/3; cre, n = 7/3; RIM1αβ$^{f/f}$xRIM2αβγ$^{f/f}$: control, n = 9/3; cre, n = 9/3.

GFP-fusion proteins to monitor the efficiency of lentiviral infection (21, 22). We only analyzed cultures in which all neurons were infected. In this manner, we analyzed RIM-deficient and control neurons that were identical except for the acute deletion of RIM proteins, which minimizes problems caused by differences in genetic backgrounds or by compensation during embryonic development (4). We will refer to neurons from conditional *Rims1* or *Rims2* KO mice as RIM1- or RIM2-deficient neurons, whereas neurons from conditional *Rims1/2* double KO mice will be called RIM1/2 double-deficient neurons.

RIMs localize Ca^{2+} influx to active zones adjacent to the sites of synaptic vesicle exocytosis by tethering Ca^{2+} channels via their PDZ domains and PxxP sequences (14, 18), and they additionally modulate Ca^{2+}-channel function, possibly via an indirect interaction with β4 subunits (15, 16, 23). To determine the redundancy among RIM isoforms in supporting Ca^{2+}-triggered neurotransmitter release and in sustaining presynaptic Ca^{2+} influx, we monitored the Ca^{2+} dependence of neurotransmitter release. We previously showed that in experiments measuring the size of IPSCs as a function of the extracellular Ca^{2+} concentration ($[Ca^{2+}]_{ex}$), one can differentiate between parameters governing the overall release process as monitored by the IPSC amplitude (which depends on properties such as vesicle docking and priming in addition to Ca^{2+} triggering) and parameters determining the Ca^{2+} dependence of release (which depends on the specific properties of the Ca^{2+}-triggering reaction, such as Ca^{2+} influx into the nerve terminal, the Ca^{2+}-sensor synaptotagmin, SNARE-complex assembly, and intracellular Ca^{2+} dynamics; see refs. 14, 24, and 25). Moreover, we showed that in the case of RIM1/2 double-deficient neurons, the decrease in overall IPSC amplitude is due to changes in multiple presynaptic parameters, but that the impairment in the Ca^{2+} dependence of release, as monitored by its apparent $[Ca^{2+}]_{ex}$ affinity, is due to changes in presynaptic Ca^{2+} influx during an action potential (14, 18). Thus, measurements of the IPSC amplitude as a function of $[Ca^{2+}]_{ex}$ can be used in RIM-deficient neurons to monitor overall release and Ca^{2+} influx.

We first measured the IPSC amplitude in RIM1- and RIM2-deficient and in RIM1/2 double-deficient neurons as a function of $[Ca^{2+}]_{ex}$ (Fig. 1 *B* and *C*). At all $[Ca^{2+}]_{ex}$, we observed a modest decrease in the IPSC amplitude in neurons lacking either only RIM1 or RIM2 (~20–30%), and a massive decrease in RIM1/2 double-deficient neurons (~75%). Thus, both *Rims* genes contribute to release.

We then normalized the IPSC amplitudes to that observed at 10 mM $[Ca^{2+}]_{ex}$ and fitted the data of individual experiments to a Hill function (24). RIM1- or RIM2-deficient neurons exhibited no change in the $[Ca^{2+}]_{ex}$ dependence of release, evidenced by the complete overlap between the fitted curves from KO and control neurons (Fig. 1*C*, *Lower*). However, and similar to what we showed before (14), RIM1/2 double-deficient neurons displayed a shift of the $[Ca^{2+}]_{ex}$ dependence of release to higher Ca^{2+} concentrations (Fig. 1*C*). The Hill function fits revealed that RIM1/2 double-deficient neurons exhibited a twofold increase in the half-maximal effective extracellular Ca^{2+} concentration (EC_{50}) for release, consistent with a loss of Ca^{2+} channels from the active zone, but did not uncover a change in the apparent Ca^{2+} cooperativity n of release (Fig. 1*D*). Thus, the *Rims1* and *Rims2* genes can fully compensate for each other in recruiting Ca^{2+} channels to active zones.

The speed and synchrony of IPSCs in cultured hippocampal neurons depend on presynaptic Ca^{2+} influx and are impaired in RIM1/2 double-deficient neurons (14, 18). When we analyzed the rise times and synchrony of single IPSCs, we found that similar to the Ca^{2+} dependence of release, each single *Rims1* or *Rims2* gene deletion had no effect on either parameter (Fig. 2). In contrast, the deletion of both genes produced a major change in both parameters. Moreover, a similar pattern of redundancy was found for the time constants of release as measured by fits of a two-component exponential function to the IPSCs (26) (Fig. S1).

In summary, RIM proteins are highly redundant functionally in mediating the Ca^{2+} dependence, speed, and synchrony of release, such that individual RIM proteins can largely provide all of the function needed. Strikingly, however, *Rims* genes exhibit different degrees of redundancy for different synaptic parameters,

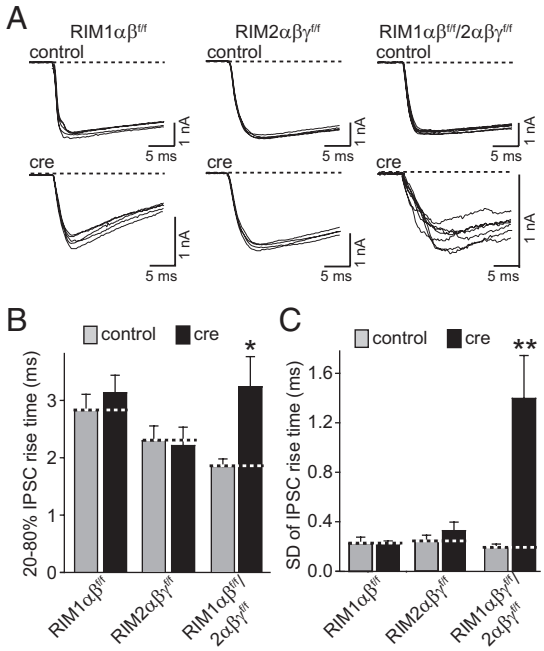

Fig. 2. Kinetic analysis of IPSCs in RIM-deficient neurons. Release was measured in response to single action potentials in cultured RIM1αβ$^{f/f}$, RIM2αβγ$^{f/f}$, and RIM1αβ$^{f/f}$/RIM2αβγ$^{f/f}$ neurons expressing inactive (control) or active cre-recombinase (cre). (*A*) Sample traces of the initial phase of isolated evoked IPSCs in floxed RIM1αβ$^{f/f}$, RIM2αβγ$^{f/f}$, and RIM1αβ$^{f/f}$/RIM2αβγ$^{f/f}$ neurons expressing inactive (control) or active cre recombinase (cre). Each trace shows five consecutive sweeps from the same neuron; note the different *y* scale for the different conditions. (*B* and *C*) Analyses of 20–80% rise time (*B*) and of the SD of the 20–80% rise time (*C*) as a measure of synchrony in control and RIM-deficient neurons. Data shown are means ± SEMs, statistical significance (*$P < 0.05$; **$P < 0.01$) was determined by Student's *t* test (*D*). RIM1αβ$^{f/f}$: control, *n* = 15 cells in 3 independent batches of cultures; cre, *n* = 15/3; RIM2αβγ$^{f/f}$: control, *n* = 12/3; cre, *n* = 14/3; RIM1αβ$^{f/f}$xRIM2αβγ$^{f/f}$: control, *n* = 10/3; cre, *n* = 11/3.

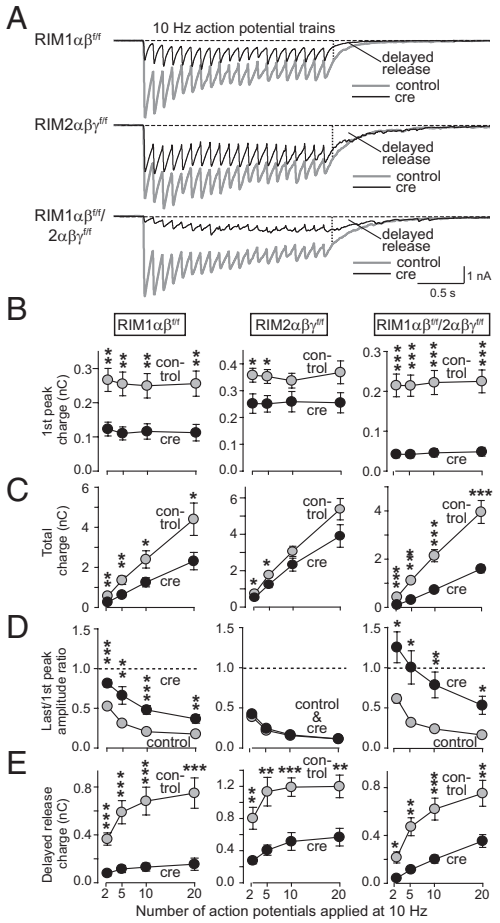

Fig. 3. Comparative analysis of the effects of single and double RIM1α/β and RIM2α/β/γ deletions on release induced by 10-Hz stimulus trains. Release was measured in response to trains with 2–20 action potentials that were elicited by focal stimulation at 10 Hz in RIM1αβ$^{f/f}$, RIM2αβγ$^{f/f}$, and RIM1αβ$^{f/f}$/RIM2αβγ$^{f/f}$ neurons expressing inactive (control) or active cre recombinase (cre). (*A*) Sample traces of IPSCs in response to a train of 20 stimuli. (*B*) Summary graphs of the synaptic charge transfer evoked by the first action potential in trains of 2, 5, 10, and 20 action potentials. (*C*) Summary graphs of the total charge transfer during each entire stimulus train. (*D*) Plots of the ratios of the evoked amplitudes of the last to the first response in each train. (*E*) Summary graphs of delayed release, measured as the charge transfer starting 100 ms after the last action potential was applied in the train. Data are shown as means ± SEMs. Statistical significance in (*B–E*): *$P < 0.05$; **$P < 0.01$; ***$P < 0.001$ calculated by one-way ANOVA (RIM1αβ$^{f/f}$: control, *n* = 6 cells in 3 independent batches of cultures; cre, *n* = 6/3; RIM2αβγ$^{f/f}$: control, *n* = 9/3; cre, *n* = 9/3; RIM1αβ$^{f/f}$/RIM2αβγ$^{f/f}$: control, *n* = 10/3; cre, *n* = 14/3).

such that they completely compensate for each other in sustaining normal Ca^{2+} influx at the active zone, but only partially in mediating overall Ca^{2+}-triggered release.

Role of RIM Proteins in Different Forms of Evoked and Spontaneous Release. We measured synaptic responses during and after trains of 2–20 stimuli applied at 10 Hz (Fig. 3*A*). During a stimulus train, residual Ca^{2+} accumulates in presynaptic nerve terminals but vesicles in the RRP become depleted. We measured four parameters: (*i*) the synaptic charge transfer induced by the first action potential to monitor synchronous release (Fig. 3*B*), (*ii*) the charge transfer transmitted during the entire train to monitor overall release (Fig. 3*C*), (*iii*) the ratio of the last to first IPSC amplitudes to monitor short-term plasticity (Fig. 3*D*), and (*iv*) the synaptic charge transfer during "delayed release" (a form of asynchronous neurotransmitter release that is defined as starting 100 ms after the last action potential (Fig. 3*E*; ref. 27).

Both the RIM1 and the RIM2 single KOs impaired release throughout the train independent of the stimulus number, although the RIM1/2 double KO had a much more severe effect (Fig. 3 *A–C*). Moreover, both the RIM1 single KO and the RIM1/RIM2 double KO altered short-term plasticity by facilitating release, as would be expected with a decreased release probability. The RIM2 single KO had no effect, although it did exhibit a decrease in release (Fig. 3 *B* and *D* and Fig. S2). Interestingly, both single RIM KOs dramatically impaired delayed release, with the RIM1/2 double KO being no more deleterious to delayed release than each single KO (Fig. 3*E*). This result indicates that delayed release depends more on the release machinery (which is affected in single KOs) than on Ca^{2+} influx (which is not).

We next characterized spontaneous neurotransmitter release by measuring miniature excitatory postsynaptic currents and inhibitory postsynaptic currents (mEPSCs and mIPSCs, respectively; Fig. S3). Consistent with previous studies (19), we find that the deletion of RIM1 or of RIM2 leads to a reduction of the mEPSC and mIPSC frequencies (Fig. S3). The average amplitudes of mEPSCs and mIPSCs were unchanged, although there were small deviations in the cumulative distribution of mIPSC amplitudes. These data suggest a dose-dependent effect of the RIM deletions on spontaneous presynaptic neurotransmitter release, with no major changes in postsynaptic neurotransmitter reception.

Priming is a process at the presynaptic active zone that transforms vesicles into a ready-to-fuse state. To evaluate the

effect of RIM deletions on synaptic vesicle priming, we measured postsynaptic responses evoked by a local application of hypertonic sucrose (0.5 M) for 30 s (28). In RIM1/2 double-deficient neurons, the RRP is massively decreased because RIM proteins mediate synaptic vesicle priming by disinhibiting inactive Munc13 homodimers (14, 19, 29). We here found that similar to evoked IPSCs and spontaneous release, deletion of individual RIM genes decreased the RRP size (Fig. S4), although the size of the decrease is less than that observed with the double deletion (14, 19, 29). This experiment suggests that RIM1 and RIM2 promote priming in an additive fashion and cannot compensate in priming for each other's loss.

RIM2γ Modulates Ca^{2+}-Channel Properties in Vitro but Does Not Contribute Significantly to RIM Function in Vivo. In addition to their Ca^{2+}-channel tethering function via their PDZ domains (14), RIMs have been shown to inhibit voltage-dependent inactivation of Ca^{2+}-channel opening via their C_2B domains (15, 16, 23). Thus, we set out to test whether this mechanism contributes to the neurotransmitter release phenotype produced by the RIM1/2 double KO.

We first coexpressed in transfected HEK293T cells the α1-subunits of rat N-type ($Ca_V2.2$) and L-type ($Ca_V1.2$) Ca^{2+} channels with the auxiliary rat α2δ and the human β4 subunits and with either control vector DNA or expression vectors encoding full-length rat RIM1α or RIM2γ (a RIM2 isoform that consists of only the RIM2 C_2B-domain preceded by a short, RIM2γ-specific sequence (Fig. 1*A*; refs. 3, 5, and 14). We then measured the electrophysiological properties of the Ca^{2+} channels as a function of the coexpressed RIM proteins.

In agreement with previous results (15, 16, 23), cotransfection of RIM1α or of RIM2γ with the N-type Ca^{2+} channels did not alter current-voltage (I-V) relationship and activation of N-type Ca^{2+} channels (Fig. 4 *A–E*), but significantly shifted the inactivation curve to higher voltage (Fig. 4 *F* and *G*). Because this effect was equally observed with RIM1α and RIM2γ, the RIM C_2B-domain must be responsible for RIM's effect on Ca^{2+}-channel inactivation. However, neither RIM1α nor RIM2γ altered L-type Ca^{2+}-channel inactivation (Fig. 4 *H–N*). Because the only difference between the experiments with the N- and L-type Ca^{2+} channels is the identity of the α1-subunit, RIM proteins likely act directly on the α1-subunit of the N-type Ca^{2+} channel to change its inactivation properties (Fig. 4).

Finally, we tested whether the loss of Ca^{2+}-channel modulation by RIMs contributes to the RIM1/2 double KO phenotype. However, we found that RIM2γ—which fully mediates the modulation of Ca^{2+}-channel inactivation by RIM proteins (Fig. 4)—was unable to rescue any facet of the RIM1/2 double KO phenotype (Fig. 5). Specifically, RIM2γ did not increase single evoked IPSCs or the Ca^{2+} dependence of release (Figs. 5 *A–D*). Moreover, RIM2γ did not ameliorate the decrease in the RRP observed in RIM1/2 double-deficient neurons (Fig. 5 *E* and *F*). This lack of rescue effect by RIM2γ is in strong contrast to the release-boosting effect of the double C_2A/B-domain fragment of RIM1 that we reported (14), indicating that the loss of the inhibition of Ca^{2+}-channel inactivation by the RIM C_2B-domain does not substantially contribute to the overall phenotype of the RIM1/2 double KO mice.

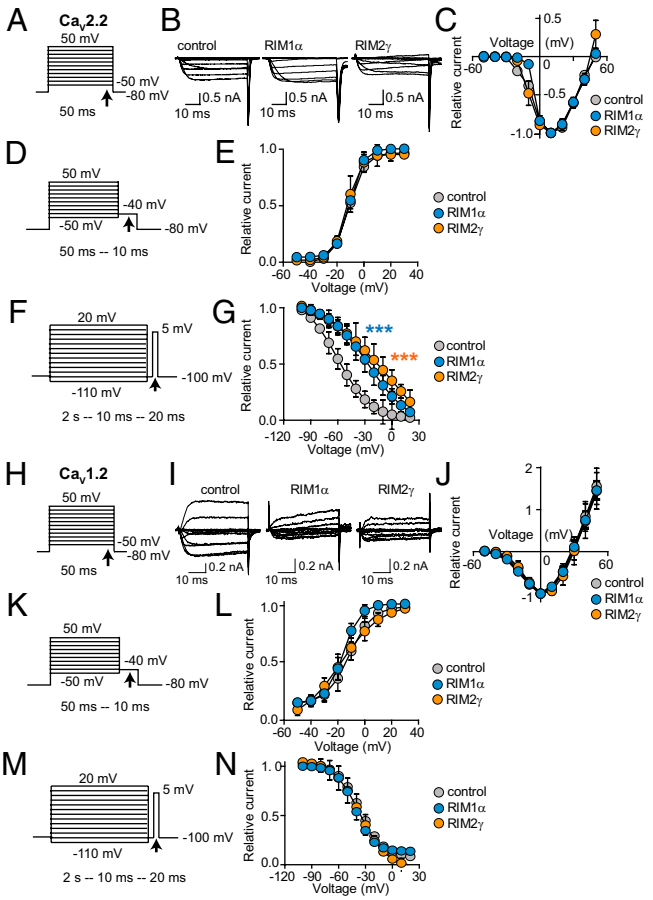

Fig. 4. Effects of RIM1α and RIM2γ on N-type and L-type Ca^{2+} channels in HEK293T cells. HEK293T cells were transfected with Ca^{2+}-channel α-subunits (N-type, $Ca_V2.2$, A-G; L-type, $Ca_V1.2$, H-N), auxiliary β4b and α2δ subunits, and either RIM1α or RIM2γ. (*A–C*) Experimental protocol (*A*), sample traces (*B*), and summary (*C*) of the current-voltage relationship of N-type $Ca_V2.2$ channels in the absence or presence of RIM1α or RIM2γ (control, n = 15 cells in 4 batches of independent transfections; RIM1α, n = 10/4; RIM2γ, n = 13/3). (*D* and *E*) Experimental protocol (*D*) and summary plot (*E*) of the activation curve of N-type $Ca_V2.2$ channels in the absence or presence of RIM1α or RIM2γ (control, n = 12/4; RIM1α, n = 13/5; RIM2γ, n = 12/4). (*F* and *G*) Experimental protocol (*F*) and summary data (*G*) of the inactivation curve (control, n = 9/4; RIM1α, n = 9/5; RIM2γ, n = 9/4) of $Ca_V2.2$ channels in the absence or presence of RIM1α or RIM2γ. (*H–J*) Experimental protocol (*H*), sample traces (*I*), and summary (*J*) of the current-voltage relationship of L-type $Ca_V1.2$ channels in the absence or presence of RIM1α or RIM2γ (control, n = 11/ 3; RIM1α, n = 14/4; RIM2γ, n = 7/3). (*K* and *L*) Experimental protocol (*K*) and summary plot (*L*) of the activation curve of L-type $Ca_V1.2$ channels in the absence or presence of RIM1α or RIM2γ (control, n = 12/3; RIM1α, n = 13/3; RIM2γ, n = 12/3). (*M* and *N*) Experimental protocol (*M*) and summary data (*N*) of the inactivation curve (control, n = 7/3; RIM1α, n = 6/3; RIM2γ, n = 10/4) of $Ca_V1.2$ channels in the absence or presence of RIM1α or RIM2γ. Data shown are means ± SEMs, statistical significance: ***$P < 0.001$ for RIM1α and RIM2γ compared with control determined by two-way ANOVA. No other significant differences in two-way ANOVA analyses were observed.

Discussion

Many proteins are expressed in multiple isoforms encoded by similar genes, prompting the question of the redundancy vs. uniqueness of the various functions of the genes. Here, we have addressed this issue for the different functions of RIM proteins in neurotransmitter release. With redundancy, we mean the existence of parallel pathways to achieve a function, either by expression of a homologous gene or by a molecularly distinct mechanism, whereas with compensation we mean the increased use of a redundant pathway whose increased use is induced by a gene's mutation. In a way, compensation is a variant of redundancy that operates when the default pathway for a function is inactivated. RIM proteins are central components of the active zone with essential functions in neurotransmitter release and presynaptic plasticity (4, 6, 9, 10, 15, 16, 30, 31; Table S1). Using conditional KO mice in which expression of the *Rims1* or *Rims2* gene or both can be acutely inactivated by cre-recombination, we have explored the nature, extent, and isoform dependence of these functions. We answered two major questions.

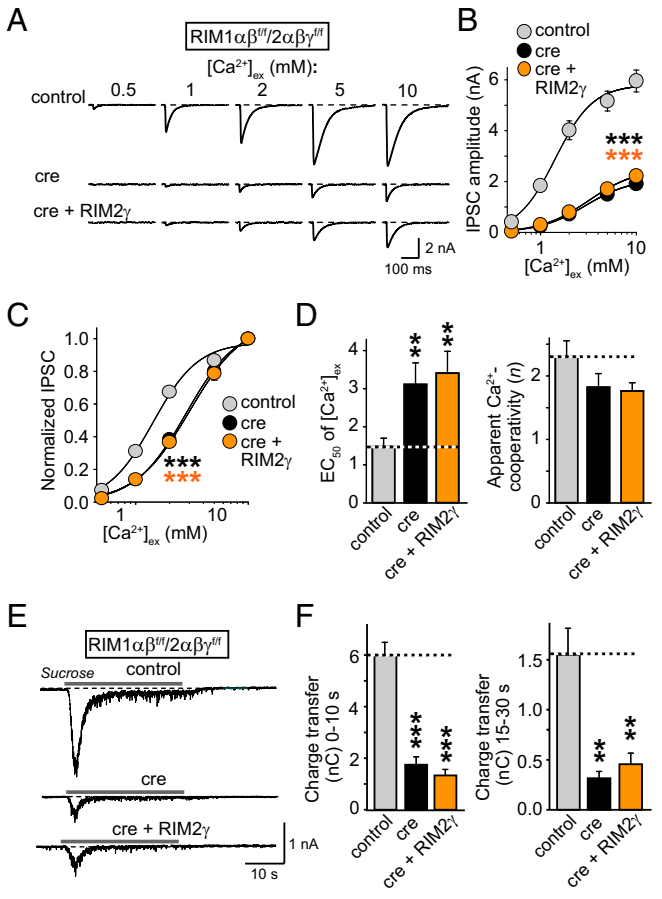

Fig. 5. Effect of RIM2γ on the extracellular Ca^{2+} dependence of neurotransmitter release and on the priming of synaptic vesicles. Release was measured in RIM1αβ$^{f/f}$/RIM2αβγ$^{f/f}$ neurons expressing inactive (control) or active cre-recombinase (cre), or cre + RIM2γ expressed bicistronically from the same lentivirus as described (14, 19, 21). (*A*) Sample traces of single evoked IPSCs, the extracellular Ca^{2+}-concentration ($[Ca^{2+}]_{ex}$) was varied as indicated. (*B*) Summary graphs of absolute IPSC amplitudes. (*C*) Summary graphs of normalized IPSC amplitudes normalized to the response at 10 mM $[Ca^{2+}]_{ex}$. (*D*) EC_{50} (*Left*; $[Ca^{2+}]_{ex}$ that elicits 50% of the maximal response) and apparent Ca^{2+} cooperativity of release (*Right*), determined by fitting each single experiment shown in *B* to a Hill function (24). (*E*) Sample traces of IPSCs evoked by 0.5 M sucrose application from RIM1αβ$^{f/f}$/RIM2αβγ$^{f/f}$ neurons after cre and control infection, or infection with a virus expressing cre + RIM2γ. (*F*) Summary graphs of the synaptic charge transfer during the initial (1–10 s) and the steady-state (15–30 s) phases of the sucrose response are shown. Data shown are means ± SEMs; statistical significance: $^{**}P < 0.01$; $^{***}P < 0.001$ was determined by one-way ANOVA (*B* and *C*) or Student's *t* test (*D* and *F*), with control, $n = 5/2$; cre, $n = 5/2$; cre + RIM2γ; $n = 4/2$ for *B*–*D*; and control, $n = 8/3$; cre, $n = 10/3$; cre + RIM2γ, $n = 10/3$ for *F*.

First, we tested whether RIM proteins are similarly redundant for different functions in release, e.g., their actions in vesicle priming, exocytosis, and Ca^{2+}-channel tethering. Our data indicate that the RIM1 and RIM2 genes exhibit surprisingly different degrees of redundancy for different functions (Table 1). Whereas the single RIM KOs significantly impaired spontaneous and evoked neurotransmitter release, they had no effect on the parameters of release that depend on Ca^{2+} influx—the apparent Ca^{2+} affinity, synchrony, and speed of release (Fig. 1–Fig. 3). These parameters were only changed upon deletion of both RIM genes, with large effect sizes, confirming the major function of RIM proteins in localizing Ca^{2+} influx to active zones (14, 18). In contrast, RIM1 and RIM2 separately contribute to the amount of release and synaptic vesicle priming at inhibitory hippocampal synapses in a dose-dependent manner (Fig. 1–Fig. 3 and Figs. S1–S4). Thus, RIMs operate additively during vesicle priming, and neither RIM gene can compensate completely for the loss of the other in priming.

Second, given that RIMs were implicated in two different functions affecting Ca^{2+} channels—namely Ca^{2+}-channel tethering and the modulation of their inactivation kinetics—we asked whether these functions synthetically and/or redundantly contribute to the overall role of RIM proteins in neurotransmitter release. RIM proteins recruit Ca^{2+} channels to active zones (14, 18) and prolong Ca^{2+}-channel opening via inhibiting voltage-dependent Ca^{2+}-channel inactivation. It was proposed that the latter effect involves binding of the RIM C_2B domain to auxiliary Ca^{2+}-channel β-subunits, which was suggested to also "dock" vesicles to Ca^{2+} channels (15, 16, 23). Here, we show that the RIM C_2B-domain modulates Ca^{2+}-channel inactivation in vitro, but probably does so by a mechanism dependent on the α-subunit of the Ca^{2+} channels because the modulation was not observed for L-type Ca^{2+} channels (Fig. 4). Most importantly, we observed that RIM2γ, which potently decreased Ca^{2+}-channel inactivation in transfected HEK293T cells, did not detectably rescue any aspect of the phenotype of RIM1/2 double KO neurons. Thus, the activity of the RIM C_2B-domain in modulating voltage-dependent Ca^{2+}-channel inactivation does not significantly contribute to the synaptic functions of RIM proteins. This result is in strong contrast to the major role of RIM proteins in tethering Ca^{2+} channels to the active zone via their PDZ domain and via RIM-BPs (14, 18), and of a RIM fragment containing both of its two C_2 domains to boost neurotransmitter release in RIM1/2 double-deficient neurons without enhancing Ca^{2+} influx (14).

Experimental Procedures

Mice. Floxed RIM1αβ and RIM2αβγ conditional KO mice (4, 14) were bred as homozygous single or double mutant mice for RIM1 (RIM1αβ$^{f/f}$), RIM2 (RIM2αβγ$^{f/f}$), or both (RIM1αβ$^{f/f}$/RIM2αβγ$^{f/f}$). All experiments were performed according to institutional guidelines.

Neuronal Cultures and Lentiviruses. Primary hippocampal neuronal cultures were prepared from newborn pups of RIM1αβ$^{f/f}$, RIM2αβγ$^{f/f}$, or RIM1αβ$^{f/f}$/RIM2αβγ$^{f/f}$ mice according to standard protocols (4, 21). Hippocampi of newborn offsprings were isolated within 24 h after birth, digested with papain or trypsin, and plated onto coated glass coverslips. Glial growth was controlled by continuous presence of cytosine arabinoside starting at 2–3 d in vitro (DIV). Lentiviruses expressing GFP-tagged cre-recombinase, a recombination deficient deletion mutant thereof, or cre-recombinase and RIM2γ by use of bicistronic expression (14, 19, 21) were generated in transfected HEK293T cells as described (21, 22), and the HEK293T cell supernatant containing the lentiviruses was harvested 48 h after transfection. Cell debris was removed by centrifugation (5 min at 750 × *g*), and neuronal cultures were infected with freshly prepared lentiviruses contained in the HEK293T cell supernatant 3–5 d after plating.

Electrophysiology in Neurons. Whole-cell patch-clamp recordings were performed in cultured hippocampal neurons at DIV 13–15 as described (14, 20, 27). The extracellular solution contained 140 mM NaCl, 4 mM KCl, 2 mM $CaCl_2$, 2 mM $MgCl_2$, 10 mM Hepes-NaOH at pH 7.3, and 10 mM glucose, with 315 mOsm. Glass pipettes (3–5 MΩ) were filled with an internal solution containing 145 mM CsCl, 5 mM NaCl, 10 mM Hepes-CsOH at pH 7.3, 10 mM EGTA, 4 mM MgATP, and 0.3 mM Na_2GTP, with 305 mOsm. IPSCs were elicited by a local stimulation electrode in the presence of 10 μM CNQX and 50 μM D-APV. For RRP measurements, 0.5 M hypertonic sucrose was applied by gravity for 30 s in the presence of 1 μM TTX, 20 μM CNQX, and 50 μM APV. For Ca^{2+} titrations, IPSCs were evoked at 0.1–0.2 Hz in neurons perfused at 0.5, 1, 2, 5, and 10 mM extracellular Ca^{2+} ($[Ca^{2+}]_{ex}$) in 2 mM $[Mg^{2+}]_{ex}$. The order of perfusion was alternated but always began and ended with 2 mM $[Ca^{2+}]_{ex}$. Neurons showing more than 15% deviation in amplitude size between the initial and the final IPSC measurement at 2 mM $[Ca^{2+}]_{ex}$ were excluded from the analysis. Amplitudes were plotted as a function of $[Ca^{2+}]_{ex}$ and fitted with the Hill equation $[I = I_{max}/1 + (EC_{50}/[Ca^{2+}]_{ex})^n]$, where I is the amplitude, I_{max} is the maximal current, EC_{50} the $[Ca^{2+}]_{ex}$ at which I is 50% of I_{max}, and n the apparent Ca^{2+} cooperativity; no constraints were used for the

Table 1. Summary of redundancy among RIM1 and RIM2 gene functions

Parameter	RIM1αβ KO	RIM2αβγ KO	RIM1αβ/ 2αβγ DKO	Source or refs.
Mini EPSC amplitude	↔	↔	↔	Fig. S3, refs. 4, 19
Mini EPSC frequency	↓	↓	↓↓	Fig. S3, refs. 4, 19
Mini IPSC amplitude	↔	↔	↔	Fig. S3, refs. 4, 19
Mini IPSC frequency	↓	↓	↓↓	Fig. S3, refs. 4, 19
Evoked IPSC amplitude	↓	↓	↓↓	Fig. 1–Fig. 3, refs. 4, 14, 19
Evoked EPSC amplitude	n.d.	n.d.	↓↓	Ref. 14
Synchronization of release	↔	↔	↓↓	Fig. 2, ref. 14
Ca^{2+} responsiveness				
$[Ca^{2+}]_{ex}$ EC_{50}	↔	↔	↓↓	Fig. 1, ref. 14
$[Ca^{2+}]_{ex}$ n	↔	↔	↔	Fig. 1, ref. 14
RRP	↓	↓	↓↓	Fig. S4, refs. 14, 19

Data summarize the results obtained in the cited references or figures. ↔, no change; ↓, decrease; n.d., not determined.

fittings. mEPSCs and mIPSCs were recorded in the presence of 1 μM TTX plus either 50 μM picrotoxin and 50 μM APV (mEPSCs) or 10 μM CNQX and 50 μM D-APV (mIPSCs), respectively. Data were acquired with a multiclamp 700B amplifier by using pClamp9 sampled at 10 kHz. For all electrophysiological experiments, the experimenter was blind to the condition/genotype of the cultures analyzed.

Electrophysiology in Transfected HEK293T Cells. HEK cells were transfected with lipofectamine with the following Ca^{2+}-channel subunits: rat pCMV-$Ca_v2.2$ or rat pCDNA4-$Ca_v1.2$; rat pCDNA3-α2δ; and human pCDNA3-β4b. In addition, either pCMV-RIM1α or pCMV-RIM2γ (and pCMV-mVenus as a marker in all conditions) were cotransfected. Whole-cell recordings were carried out at room temperature (22–24 °C) 48 h after transfection with glass pipettes at 2–4 MΩ resistance. Currents were sampled at 10 kHz and filtered at 2 kHz. Leak currents were subtracted by a –P/4 protocol. The external solution contained 10 mM $BaCl_2$, 140 mM TEA-Cl, 10 mM Hepes, 10 mM glucose (pH adjusted to 7.4 with tetraethylammonium-OH). The internal pipette solution contained 135 mM $CsMeSO_3$, 5 mM CsCl, 0.5 mM EGTA, 5 mM $MgCl_2$, 4 mM $ATPNa_2$ and 10 mM Hepes (pH adjusted to 7.2 with CsOH). For current-voltage (I-V) curve and activation curve recordings, currents were evoked from a holding potential at –80 mV by 50 ms depolarizations ranging from −50 mV to +50 mV in 10-mV increments at 1 s intervals. The I-V curve was normalized to the peak current. The activation curve was normalized to the tail current after a 30-mV depolarization. For measuring channel inactivation, the currents were evoked by a 20-ms depolarization to 5 mV after 10-ms repolarization to −100 mV after a 2-s holding potential at −100 mV to +20 mV in 10-mV increments. Inactivation curves were normalized to the current evoked after the 2-s depolarization at −100 mV. Activation and inactivation curves were fitted by Boltzmann's charge-voltage equation.

Data Analyses. All data are shown as means ± SEM. Statistical significance was determined as indicated in the figure legends.

ACKNOWLEDGMENTS. We thank Han Ly and Iza Kornblum for excellent technical assistance, and members of the T.C.S. laboratory for comments and advice. This work was supported by National Institutes of Health Grants POMH086403 and RO1NS077906 (to T.C.S.) and DA029044 (to P.S.K.).

1. Gundelfinger ED, Fejtova A (October 24, 2011) Molecular organization and plasticity of the cytomatrix at the active zone. *Curr Opin Neurobiol*, 10.1016/j.conb.2011.10.005.
2. Kaeser PS (2011) Pushing synaptic vesicles over the RIM. *Cell Logist* 1:106–110.
3. Wang Y, Südhof TC (2003) Genomic definition of RIM proteins: Evolutionary amplification of a family of synaptic regulatory proteins(small star, filled). *Genomics* 81:126–137.
4. Kaeser PS, et al. (2008) RIM1alpha and RIM1beta are synthesized from distinct promoters of the RIM1 gene to mediate differential but overlapping synaptic functions. *J Neurosci* 28:13435–13447.
5. Wang Y, Sugita S, Sudhof TC (2000) The RIM/NIM family of neuronal C2 domain proteins. Interactions with Rab3 and a new class of Src homology 3 domain proteins. *J Biol Chem* 275:20033–20044.
6. Schoch S, et al. (2002) RIM1alpha forms a protein scaffold for regulating neurotransmitter release at the active zone. *Nature* 415:321–326.
7. Weimer RM, et al. (2006) UNC-13 and UNC-10/rim localize synaptic vesicles to specific membrane domains. *J Neurosci* 26:8040–8047.
8. Gracheva EO, Hadwiger G, Nonet ML, Richmond JE (2008) Direct interactions between C. elegans RAB-3 and Rim provide a mechanism to target vesicles to the presynaptic density. *Neurosci Lett* 444:137–142.
9. Koushika SP, et al. (2001) A post-docking role for active zone protein Rim. *Nat Neurosci* 4:997–1005.
10. Schoch S, et al. (2006) Redundant functions of RIM1alpha and RIM2alpha in Ca(2+)-triggered neurotransmitter release. *EMBO J* 25:5852–5863.
11. Fourcaudot E, et al. (2008) cAMP/PKA signaling and RIM1alpha mediate presynaptic LTP in the lateral amygdala. *Proc Natl Acad Sci USA* 105:15130–15135.
12. Castillo PE, Schoch S, Schmitz F, Südhof TC, Malenka RC (2002) RIM1alpha is required for presynaptic long-term potentiation. *Nature* 415:327–330.
13. Chevaleyre V, Heifets BD, Kaeser PS, Südhof TC, Castillo PE (2007) Endocannabinoid-mediated long-term plasticity requires cAMP/PKA signaling and RIM1alpha. *Neuron* 54:801–812.
14. Kaeser PS, et al. (2011) RIM proteins tether Ca2+ channels to presynaptic active zones via a direct PDZ-domain interaction. *Cell* 144:282–295.
15. Kiyonaka S, et al. (2007) RIM1 confers sustained activity and neurotransmitter vesicle anchoring to presynaptic Ca2+ channels. *Nat Neurosci* 10:691–701.
16. Uriu Y, et al. (2010) Rab3-interacting molecule gamma isoforms lacking the Rab3-binding domain induce long lasting currents but block neurotransmitter vesicle anchoring in voltage-dependent P/Q-type Ca2+ channels. *J Biol Chem* 285:21750–21767.
17. Hibino H, et al. (2002) RIM binding proteins (RBPs) couple Rab3-interacting molecules (RIMs) to voltage-gated Ca(2+) channels. *Neuron* 34:411–423.
18. Han Y, Kaeser PS, Südhof TC, Schneggenburger R (2011) RIM determines Ca^{2+} channel density and vesicle docking at the presynaptic active zone. *Neuron* 69:304–316.
19. Deng L, Kaeser PS, Xu W, Südhof TC (2011) RIM proteins activate vesicle priming by reversing autoinhibitory homodimerization of Munc13. *Neuron* 69:317–331.
20. Maximov A, Pang ZP, Tervo DG, Südhof TC (2007) Monitoring synaptic transmission in primary neuronal cultures using local extracellular stimulation. *J Neurosci Methods* 161:75–87.
21. Kaeser PS, et al. (2009) ELKS2alpha/CAST deletion selectively increases neurotransmitter release at inhibitory synapses. *Neuron* 64:227–239.
22. Ho A, et al. (2006) Genetic analysis of Mint/X11 proteins: Essential presynaptic functions of a neuronal adaptor protein family. *J Neurosci* 26:13089–13101.
23. Miki T, et al. (2007) Mutation associated with an autosomal dominant cone-rod dystrophy CORD7 modifies RIM1-mediated modulation of voltage-dependent Ca2+ channels. *Channels (Austin)* 1:144–147.
24. Fernández-Chacón R, et al. (2001) Synaptotagmin I functions as a calcium regulator of release probability. *Nature* 410:41–49.
25. Gerber SH, et al. (2008) Conformational switch of syntaxin-1 controls synaptic vesicle fusion. *Science* 321:1507–1510.
26. Pang ZP, et al. (2006) Synaptotagmin-2 is essential for survival and contributes to Ca2+ triggering of neurotransmitter release in central and neuromuscular synapses. *J Neurosci* 26:13493–13504.
27. Maximov A, Südhof TC (2005) Autonomous function of synaptotagmin 1 in triggering synchronous release independent of asynchronous release. *Neuron* 48:547–554.
28. Rosenmund C, Stevens CF (1996) Definition of the readily releasable pool of vesicles at hippocampal synapses. *Neuron* 16:1197–1207.
29. Lu J, et al. (2006) Structural basis for a Munc13-1 homodimer to Munc13-1/RIM heterodimer switch. *PLoS Biol* 4:e192.
30. Wang Y, Okamoto M, Schmitz F, Hofmann K, Südhof TC (1997) Rim is a putative Rab3 effector in regulating synaptic-vesicle fusion. *Nature* 388:593–598.
31. Yao I, et al. (2007) SCRAPPER-dependent ubiquitination of active zone protein RIM1 regulates synaptic vesicle release. *Cell* 130:943–957.